

## Seismic Monitoring of CO<sub>2</sub> Sequestration

### Investigators

Jerry M. Harris, Professor, Geophysics Department; Youli Quan, Research Associate, Geophysics Department; Chuntang Xu, Jaime Urban, Graduate Research Assistants.

### Background

In the last two annual reports on CO<sub>2</sub> storage monitoring, we discussed the feasibility of using different geophysical options for subsurface CO<sub>2</sub> monitoring, and described an innovative approach for near-continuous subsurface monitoring. We also discussed special challenges and requirements with continuous and leak detection of CO<sub>2</sub>. We chose seismic methods for subsurface monitoring primarily because they are broadly applicable in a variety of geological settings and sensitive to changes in CO<sub>2</sub> saturation. To further develop seismic methods, for this particular application, we have proposed adaptive sparse data acquisition to address the problem of cost-effective time-lapse monitoring. We focused our work on leak detection and have proposed data gathering and processing concepts for dynamic imaging and model-based inversion. Developments reported in previous reports included a suite of seismic modeling tools to simulate monitoring and a small-scale field example on seismic monitoring of enhanced coal bed methane production. The concept of affordable permanent sensors and sparse data acquisition has been demonstrated and reported in a recent publication [8]. The results of this demonstration, using an ocean bottom cable, provide further evidence for the viability of near-continuous monitoring strategy for CO<sub>2</sub> storage.

This report presents three pieces of work completed over the past year:

- Estimating flow properties of porous media with a model for dynamic diffusion, which helps to understand how acoustic behave in porous media and provides realistic parameters for simulation.
- 3-D seismic simulations of monitoring for CO<sub>2</sub> storage, which provides data for testing the proposed monitoring strategies, e.g., sparse 3-D seismic surveys and dynamic imaging.
- Leak detection using simple cross arrays, an example with simulated data.

### Results

*Estimating Flow Properties of Porous Media with a Model for Dynamic Diffusion* - In geological sequestration, CO<sub>2</sub> is stored in the pore space of rocks. In order to know if changes caused by the injected CO<sub>2</sub> are observable with seismic methods, we need to study the porous medium and its response to seismic signals. We have developed a dynamic diffusion model to use with the DARS laboratory method to estimate the properties of rock samples. The porous properties studied include effective compressibility and permeability. Harris et al. [1] described the fundamentals of DARS technique and applied it for acoustic attenuation estimation. The special features of DARS (Differential Acoustic Resonance Spectroscopy) include (a) low sonic frequency, and (b) ability to measure unconsolidated or irregularly shaped samples.

Consider a fluid-saturated porous sample that is subjected to a small amplitude oscillatory pressure gradient. The pressure fluctuation will cause micro fluid flow through the sample in order to release the differential pressure. This phenomenon can be described by dynamic diffusion. In cylindrical coordinates, the pressure diffusion equation for a homogeneous circular porous sample has the following form [2]:

$$\frac{1}{r} \frac{\partial}{\partial r} \left( r \frac{\partial p}{\partial r} \right) = \frac{1}{D} \frac{\partial p}{\partial t} \quad (1)$$

with  $D = k/(\phi\eta\beta)$ . Here  $\phi$  and  $k$  are porosity and permeability of the sample,  $p$  is the acoustic pressure in the fluid,  $\eta$  is the viscosity of the fluid, and  $\beta$  is the compressibility factor involving both the fluid and the solid matrix. From the solution of equation (1) and the definition of compressibility we obtain a find an expression for the effective compressibility  $\kappa_e$ :

$$\kappa_e \approx \kappa_\infty + \frac{2\kappa_f\phi}{r_o^2} \int_0^{r_o} \frac{K_o(\sqrt{i\omega/Dr})}{K_o(\sqrt{i\omega/Dr_o})} r dr, \quad (2)$$

where  $\omega$  is angular frequency of the pressure field,  $r_o$  is radius of the sample,  $\kappa_\infty$  is the high frequency compressibility of the wet sample, and  $K_o$  is the zero-order modified Bessel function of the second kind.

We tested equation (2) with lab data. The conventional ultrasonic transit time method and DARS were respectively used to measure compressibility for eight rock samples (Table 1). We also calculated the theoretical effective compressibility  $\kappa_e$  using equation (2). The ultrasonic compressibility is used as  $\kappa_m$  in the computation. The resulting compressibility, estimated three different ways, is shown in Table 2. It can be seen that the compressibility estimated by DARS is very close to that predicted by equation (2) for all samples. For low permeability samples (e.g., chalk, granite, and coal), all three methods (DARS, ultrasound, and dynamic diffusion) agree.

This test shows that the compressibility obtained from DARS is indeed an effective compressibility, and that the interaction of the fluid and the solid skeleton on permeable samples is a dynamic diffusion process. We may use this diffusion model to interpret the DARS data. As shown in equation (2),  $\kappa_e$  is a function of permeability and porosity of porous media. Therefore, DARS is suitable to investigate the flow properties of porous media.

Table 3 shows the permeability calculated using equation (2) and DARS data according to following procedure: (a) assume all the variables except permeability on the right hand of the equation are known, (b) estimate  $\kappa_e$  using DARS data, and (c) substitute the  $\kappa_e$  into the equation and solve for the permeability. For comparison, the permeability measured by gas-injection method is also listed in the table. The results by these two method matches well. We used cylindrical samples in this experiment. We

need to generalize the diffusion equation for more complicated cases, so that we can interpret irregular samples.

**Table 1:** Acoustic and flow properties of eight rock samples used in the test. The density,  $P$ -wave and  $S$ -wave velocities are measured in the dry state.

	$v_p$ (m/s)	$v_s$ (m/s)	$\rho$ (g/cc)	$\phi$ (%)	$k$ (mD)
Berea 1	2656	1650	2.101	20.85	370
Berea 2	2600	1544	2.142	28	6000
Boise	2837	1658	2.309	12	0.9
Chalk	3019	1611	1.786	34.5	2.1
Coal	2045	840	1.130	1.9	0.1
Granite	5140	2720	2.630	0.1	0
Sandstone 1	2.336	1.305	1.893	28.3	4200
Sandstone 2	2.053	1.205	1.982	24.9	1850

**Table 2:** Compressibility obtained by different methods for eight rock samples.

	$\kappa$ -ultrasound ( $\text{GPa}^{-1}$ )	$\kappa$ -DARS ( $\text{GPa}^{-1}$ )	$\kappa$ -diffusion ( $\text{GPa}^{-1}$ )
Berea 1	0.139	0.233	0.246
Berea 2	0.130	0.340	0.336
Boise	0.0988	0.117	0.104
Chalk	0.0990	0.102	0.0967
Granite	0.0230	0.0231	0.0229
Coal	0.273	0.277	0.273
Sandstone 1	0.0177	0.331	0.331
Sandstone 2	0.0121	0.327	0.328

**Table 3:** Permeability obtained by two different methods for three rock samples

	Berea 1	Sandstone 1	Sandstone 2
Permeability (mD) by gas-injection	370	4200	1850
Permeability (mD) By equation (2)	394	4230	1770

*3-D Seismic Simulations on CO<sub>2</sub> Storage Monitoring* - We proposed several new seismic monitoring strategies. Our project does not include field tests, so we use our seismic modeling tools to simulate a monitoring project in order to get a better understanding of the issues related to field implementation. We first use the finite difference simulation program to compute a set of complete time-lapse 3-D seismic surveys. Then we use them in to study different detection and imaging problems, for example, does the cross-array acquisition geometry have the potential to a detect CO<sub>2</sub> leak in a realistic geology setting, or whether dynamic imaging approach works better than the conventional stationary imaging method?

The three-dimensional finite difference (FD) simulation methods discussed in the report of last year are used to compute the time-lapse 3-D seismic surveys. In this report, we use the acoustic FD program for the simulation. The acoustic wave field is the simplest. Later, we will carry out more complicated simulations using other programs that may include *P*-wave, *S*-wave, and/or attenuation in the future.

Assume that we have the sequestration setting as shown in Figure 1. The corresponding 3-D computational grid is shown in Figure 2. We place 107 receiver arrays on the surface and one receiver array in the injection well. Four source arrays are placed on the surface. There are 428 sources in the four source arrays. At first, we calculate this relatively dense 3-D seismic data cube. Then in the analysis stage, we extract different subsets from the original data sets to test various acquisition configurations. The CO<sub>2</sub> injected into the formation causes a decrease in seismic velocity. The velocity changes will result in travel time, amplitude and reflectivity changes of the seismic waves. These seismic attributes are the observed data that will be used to image the CO<sub>2</sub>. To simulate the injection stages, we create four time-lapse models shown in Figure 3. The CO<sub>2</sub> plume grows with time. We want to track the plume growth and detect possible leaks along the fault in this monitoring project.

The FD program was run on a Linux cluster at the Stanford Center for Computational Earth and Environment Science (CEES). Each shot required about 75 minutes CPU time on an Opteron processor (embarrassing parallel by shot). There are five models, each with 428 shots, thus the total CPU time is about 2,675 hours or 111 days. We used 64 nodes in the CEES computer cluster, so the actual clock time for this simulation was 3 days, resulting in a data file of 168 GB. For a quick check on our data volume, we extracted two orthogonal zero-offset profiles from the original data sets. Figure 4 shows the amplitude differences between two time-lapse surveys. The CO<sub>2</sub> plume is clearly seen from the data display.

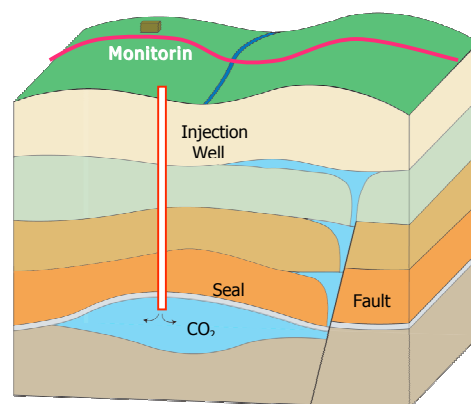


**Figure 1:** A CO<sub>2</sub> storage and monitoring project. The boundary between layers provides sealing mechanism. Leak detection is the main concern in this monitoring project. We add a fault in the model as possible leaking pathways.

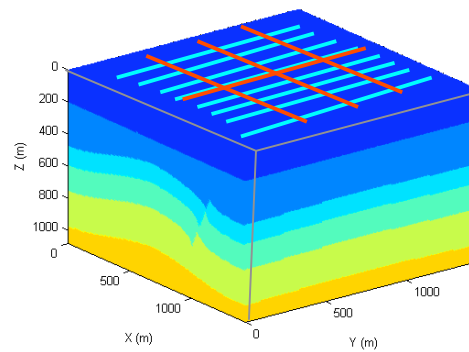


**Figure 2:** Model used for FD simulation. Blue lines are receiver arrays. There are 107 surface receiver arrays and 1 vertical receiver array in the injection borehole. Red lines represent source arrays. Three of source arrays are orthogonal to the receiver arrays, and one is parallel to the receiver arrays. The grid for this model has  $N_x = N_y = 361$  and  $N_z = 271$ .  $P$ -wave velocities, from top layer to bottom layer, are 3500, 3700, 3900, 4500, 3800, 4300 m/s. Densities are 2150, 2180, 2200, 2230, 1800, and 2200 kg/m<sup>3</sup>. A Ricker wavelet with a center frequency of 50 Hz is used in this FD computation.

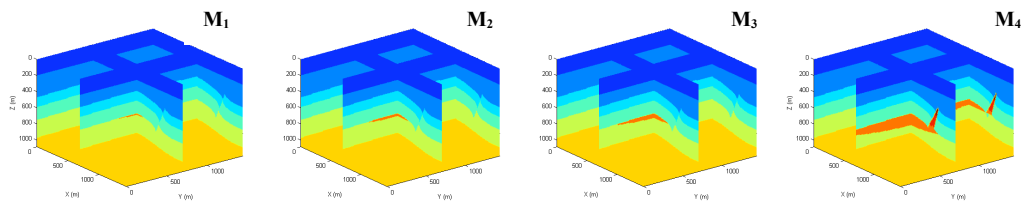


**Figure 3:** Time-lapse CO<sub>2</sub> injection models,  $M_1$ ,  $M_2$ ,  $M_3$ , and  $M_4$ . The CO<sub>2</sub> saturated area (red color in the center) has a velocity 3% less than the background velocity.

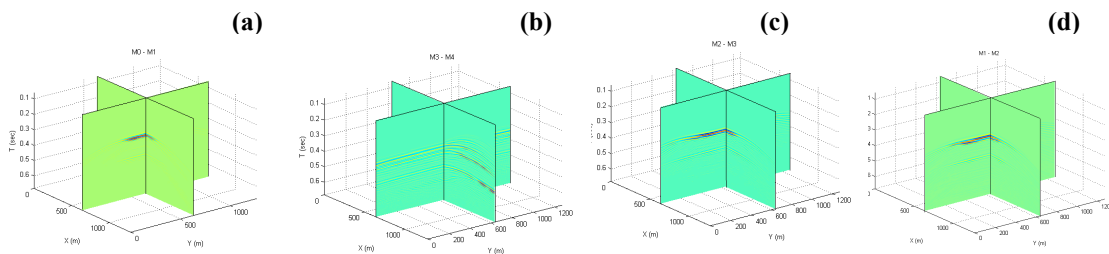


**Figure 4:** Amplitude differences between the baseline survey and time-lapse surveys. (a) Difference between Model 1 and baseline model ( $M_1-M_0$ ); (b) difference  $M_2-M_1$ ; (c) difference  $M_3-M_2$ ; and (d) difference  $M_4-M_3$ .

*Leak Detection with the Cross-array Geometry* - An example of time-lapse 3-D seismic monitoring is the cross-array (or cross-spread) acquisition geometry, an example of sparse 3-D seismic surveys [3-7]. The cross array shown in Figure 5 can be used to acquire a sparse but still true 3D seismic survey. The cross-array data can be arranged as a 3-D volume. We use 107 sources and 107 receivers. The time window of each seismic trace is 1700 points. Therefore, we have a 3-D data cube with the size of 107×107×1700. We can inspect the data cube with different orthogonal slices. Figure 6 shows a time slice, a common source gather and a common receiver gather of the baseline survey. The reflection events exhibit different shapes (e.g., moveout) on different slices. Reflections appear as circles on time slices, and as hyperbolas on common shot and common receiver slices.

When CO<sub>2</sub> is injected into the formation, it will cause changes in seismic responses, e.g., travel time and amplitude. In this simulation example we only investigate the reflection amplitude differences caused by the CO<sub>2</sub> saturation. The amplitude differences are obtained by subtracting a time-lapse survey from the baseline survey. Figure 7 shows the amplitude differences between time-lapse surveys and the baseline survey. Because the CO<sub>2</sub> is injected in the 5<sup>th</sup> layer just below the 4<sup>th</sup> interface, the seismic reflections from interfaces 1–3 are not affected by the CO<sub>2</sub> saturation. The amplitude change starts from reflection of 4<sup>th</sup> interface where CO<sub>2</sub> storage is. The CO<sub>2</sub> plume grows with time. It can be seen that the amplitude difference becomes larger due to a larger CO<sub>2</sub> storage.

As the CO<sub>2</sub> injection continues, the CO<sub>2</sub> plume reaches the fault and results a leak. CO<sub>2</sub> leaks change the seismic velocity near the fault. The velocity perturbation causes seismic diffraction. The time slice T<sub>4</sub> in Figure 7 clearly shows the diffraction pattern related to the leak along the fault. The special circular pattern is interesting. In the field data, the noise is always there, but it is random and should not generate anomaly like this pattern. This simulation shows a simple cross-spread may be capable to detect the possible leaks by looking for this kind of circular patterns.

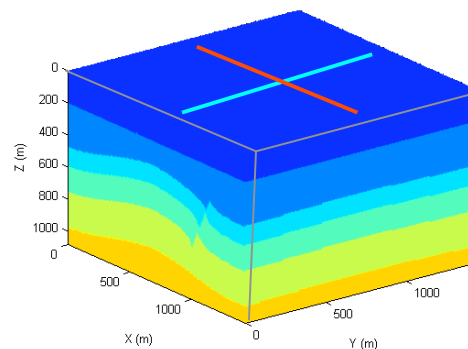


**Figure 5:** Simple cross arrays used for the CO<sub>2</sub> monitoring. This configuration is the basic 3-D seismic acquisition geometry. The red line is the source array and the blue line is the receiver array.

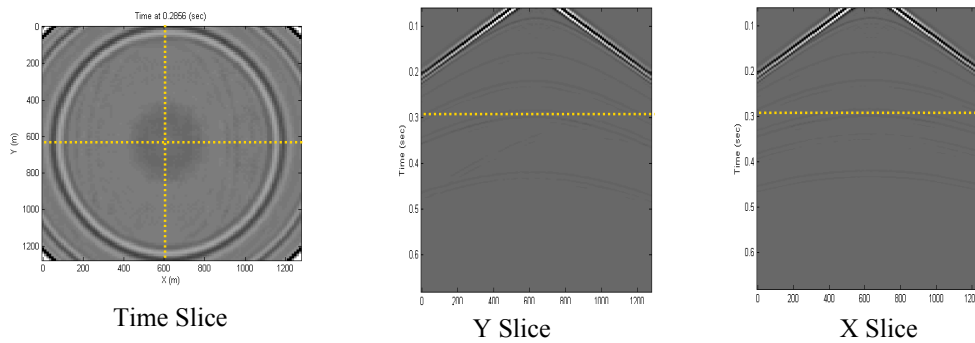


**Figure 6:** Orthogonal slices (cross array) cut from the 3-D data volume extracted from baseline model. Circles on the time slice are reflections. Yellow lines show where slices are cut.

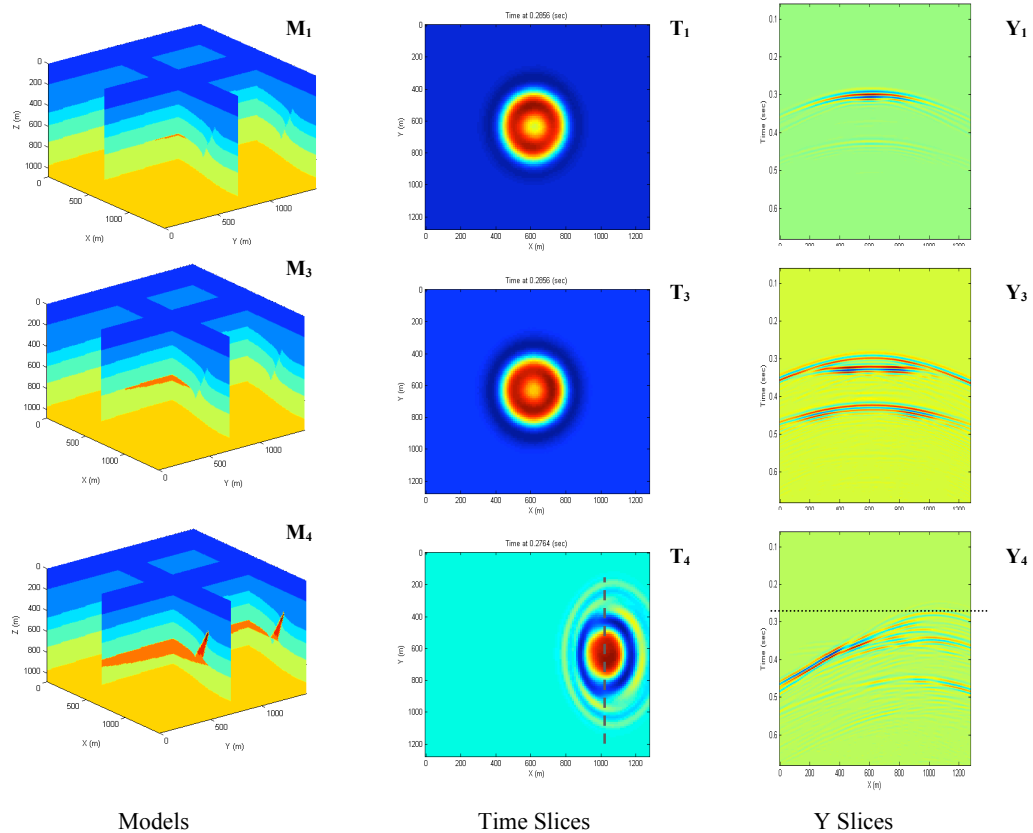


**Figure 7:** Amplitude differences between baseline survey ( $M_0$ ) and three time-lapse surveys ( $M_1$ - $M_4$ ). CO<sub>2</sub> starts leaking along the fault in Model 4. The time slice is cut at 0.2764 sec as indicated on slice  $Y_4$ . A circular anomaly above the leakage area can be seen from this time slice. It is also interesting to see that the circular contours have a linear discontinuity highlighted by the dashed line. This discontinuity is caused by the fault.

**Recent Publications**

1. Chuntang Xu, Jerry M. Harris, and Youli Quan, 2006, Estimating flow properties of porous media with a model for dynamic diffusion, SEG Expanded Abstract, in press.
2. Harris, J. H., Quan, Y. L., Xu, C. T., 2005, Differential Acoustic Resonance Spectroscopy: An experimental method for estimating acoustic attenuation in porous media, SEG Expanded Abstract, 1569-1572.

**References**

1. Harris, J. H., Quan, Y. L., Xu, C. T., 2005, Differential Acoustic Resonance Spectroscopy: An experimental method for estimating acoustic attenuation in porous media, SEG Expanded Abstract, 1569-1572.
2. Barenblatt, G.I., Entov, V.M., and Ryzhik, V.M., 1990, Theory of Fluid Flows through Natural Rocks: Dordrecht, Kluwer Academic Publishers.
3. Walton, G. G., 1972, Three-dimensional seismic method: Geophysics, 37, 417-430.
4. Vermeer, G.J.O., 1998, 3D-symmetric sampling: Geophysics, 63, No 5, 1629-1647.
5. Wapenaar, C.P.A, 1997, 3-D migration of cross-spread data: resolution and amplitude aspects: Geophysics, 62, No 4, 1220-1225.
6. Bouska, J.G, Sparse 3-D, What's in a name, Canadian Society of Exploration Geophysicists Recorder Sept. 1997.
7. Al-Ali, M., Hastings-James, R., & Al-Saad, R., 2001, Conventional and Sparse 3D: What is in between: Expanded Abstracts, SEG Annual Meeting.
8. Smit, F, M. Logtendag, P. Wilis, R. Calvert, Towards affordable permanent seismic reservoir monitoring using the sparse OBC concept.

**Contacts**

Jerry M. Harris: [harris@pangea.stanford.edu](mailto:harris@pangea.stanford.edu)  
Youli Quan: [quany@pangea.stanford.edu](mailto:quany@pangea.stanford.edu)  
Jaime Urban: [urban@pangea.stanford.edu](mailto:urban@pangea.stanford.edu)  
Chuntang Xu: [xct7015@pangea.stanford.edu](mailto:xct7015@pangea.stanford.edu)